Materials Today Nano 11 (2020) 100083

Contents lists available at ScienceDirect

Materials Today Nano

journal homepage: https://www.evise.com/profile/#/MTNANO/login

Tunable, room-temperature multiferroic Fe-$BaTiO_3$ vertically aligned nanocomposites with perpendicular magnetic anisotropy

B. Zhang [a], J. Huang [b], B.X. Rutherford [b], P. Lu [c], S. Misra [b], M. Kalaswad [a], Z. He [a], X. Gao [b], X. Sun [b], L. Li [b], H. Wang [a, b, *]

[a] School of Electrical and Computer Engineering, Purdue University, West Lafayette, IN 47907, United States
[b] School of Materials Engineering, Purdue University, West Lafayette, IN 47907, United States
[c] Sandia National Laboratories, Albuquerque, NM 87185, United States

ARTICLE INFO

Article history:
Received 22 February 2020
Received in revised form
20 April 2020
Accepted 28 April 2020
Available online 19 May 2020

Keywords:
Strain tuning
Ferroelectric
Ferromagnetic
Ordered growth

ABSTRACT

Room-temperature ferromagnetic materials with perpendicular magnetic anisotropy are widely sought after for spintronics, magnetic data storage devices, and stochastic computing. To address this need, a new Fe-$BaTiO_3$ vertically aligned nanocomposite (VAN) has been fabricated—combining both the strong room-temperature ferromagnetic properties of Fe nanopillars and the strong room-temperature ferroelectric properties of the $BaTiO_3$ matrix. Furthermore, the Fe-$BaTiO_3$ VAN allows for highly anisotropic magnetic properties with tunable magnetization and coercivity. In addition, to demonstrate the multiferroic properties of the Fe-$BaTiO_3$ system, the new metal-oxide hybrid material system has been incorporated in a multilayer stack. This new multiferroic VAN system possesses great potential in magnetic anisotropy and property tuning and demonstrates a new material family of oxide-metal hybrid systems for room-temperature multiferroic material designs.

1. Introduction

Ferromagnetic thin films are well-studied materials with a wide range of applications in electronic devices [1], especially in spintronic devices [2]. One such spintronic device, the magnetic tunnel junction, uses magnetically susceptible materials to alter electron currents to enact a resistance change [3]. For these applications, Fe, a strong ferromagnetic metal, has been well studied and integrated into a variety of spintronic devices and applications, most notably in tunnel junctions [4–6]. Traditionally, tunnel junctions have a preferred in-plane (IP) direction, but perpendicular anisotropy is highly desired for vertical tunnel junction development owing to these tunnel junctions having higher frequency, higher density, and lower power requirements. For these vertical tunnel junctions, work is needed to develop magnetic materials that exhibit a perpendicular anisotropy [7,8]. In addition, the magnetic material must present a perpendicular anisotropy with a small enough feature size allowing for integration into current integrated circuits. A promising platform that addresses both needs of creating small feature sizes and a strong perpendicular magnetic direction is vertically aligned nanocomposites (VANs) [9].

VANs enable the single-step growth of two different materials that are self-assembled into two-phase vertical structures, including pillar-in-matrix and nanocheckerboard structures [10–14]. The VAN structures present two main advantages compared with the traditional, single-phase films. First, the unique, vertical pillar structure creates highly anisotropic physical properties while accommodating significant amounts of vertical interfacial strain between the two phases. This interaction creates a large degree of property tunability [12,15–17]. Second, because VANs typically consist of two different phases, the structure introduces the possibility of combining two materials with highly desirable properties into a hybrid material. To this end, it has been shown that it is possible to combine ferroelectric oxides and ferromagnetic oxides to form multiferroic films [14,15,18,19]. Although VANs consisting of two oxide phases with desired properties have been widely demonstrated, metals have been long sought after for their strong, room-temperature, ferromagnetic properties, which are typically much stronger than their oxide counterparts. Thus, by replacing one of the oxide phases with metals, such VAN films could present strong anisotropic, metallic, physical properties under room-temperature conditions [18,20–23].

* Corresponding author.
E-mail address: hwang00@purdue.edu (H. Wang).

https://doi.org/10.1016/j.mtnano.2020.100083

Metal oxide–based VANs are uniquely equipped for multiferroic material designs owing to their ability to combine both oxide and metal phases and their respective properties. Various metal-oxide VAN systems, including Ni-CeO_2 [9], Ni-$Ba_{0.8}Zr_{0.2}Y_3$ [21], Co-$BaZrO_3$ [10], Fe-$La_{0.5}$-$Sr_{0.5}FeO_3$ [24], Au-$BaTiO_3$ [25], and Au-TiO_2 [26], have previously demonstrated that the integration of metals with oxides that have relevant room-temperature properties is possible. These metal-oxide VANs integrate either the strong plasmonic or the ferromagnetic properties of the metal phase with the oxide phase to create a highly anisotropic material system.

To achieve excellent epitaxial quality of the two phases, a new epitaxial paradigm for the two-phase nanocomposite system was used [27] for this work, i.e., the two phases shall present opposite strain states when compared with the substrate lattice. For this work, $BaTiO_3$ (BTO) was selected as the matrix, and Fe was selected as a magnetic secondary phase, as shown in Fig. 1a. With BTO being one of the most well-studied ferroelectric oxide [28–30], it has recently attracted interest owing to its non-linear optical properties [31–34] and its potential applications in different optical devices [35,36], especially wave guides [37,38].

Despite the previous work on Fe-BTO nanocomposite systems, wherein the geometries have been focused on bilayer, multilayer films with Fe on BTO or vice versa [39–42], or on embedding Fe nanoparticles within a BTO matrix [43], this work proposes integrating Fe as nanopillars into a BTO matrix. This proposed structure will allow for unprecedented strong anisotropic, ferromagnetic and ferroelectric properties, coming from Fe and BTO, respectively. In addition, this unique structure will incorporate large vertical interface strain that will enhance coupling between the Fe and BTO phases. For the Fe-BTO nanocomposite system, a large range of tunability will also be achieved, such as going from a soft ferromagnet to a hard ferromagnet, by simply controlling the Fe pillar length (i.e., film thickness), pillar density, and pillar morphology. Such tunable nanoscale ferromagnetic systems could find a wide range of applications in spintronic devices and neuromorphic computing [44] and are a promising candidate for the ongoing search for soft magnetics for stochastic computing schemes [45,46].

2. Methods and experimental procedure

The Fe-BTO target preparation was made by mixing Fe and BTO powders in a 1:1 M ratio. The mixture was pressed and sintered with inflowing Ar/H_2 into a conventional pellet target. The films were grown on single-crystalline $SrTiO_3$ (STO) (001) substrates via the pulsed laser deposition system (KrF excimer laser) (Lambda-Physik, $\lambda = 248$ nm). Multiple deposition frequencies of 2 Hz, 5 Hz, and 10 Hz were used to tune the nanostructure.

The nanostructure of the films was investigated using X-ray diffraction (XRD) (Panalytical X'Pert X-ray diffractometer). The different films were imaged by transmission electron microscopy (TEM) and scanning transmission electron microscopy (STEM), and energy dispersive X-ray spectroscopy (EDS) elemental mapping was performed by using a FEI Titan G2 80-200 STEM with a Cs probe corrector and ChemiSTEM technology (X-FEG and SuperX EDS), and additional TEM, STEM, and EDS images of the different frequencies were taken (FEI Talos-200X).

The magnetic properties of the nanocomposite thin films were analyzed both parallel (IP) and perpendicular (out-of-plane [OP]) to the film surface in the vibrating sample mode in a Magnetic Property Measurement System (MPMS 3, Quantum Design). The piezoelectric properties were measured by Bruker atomic force

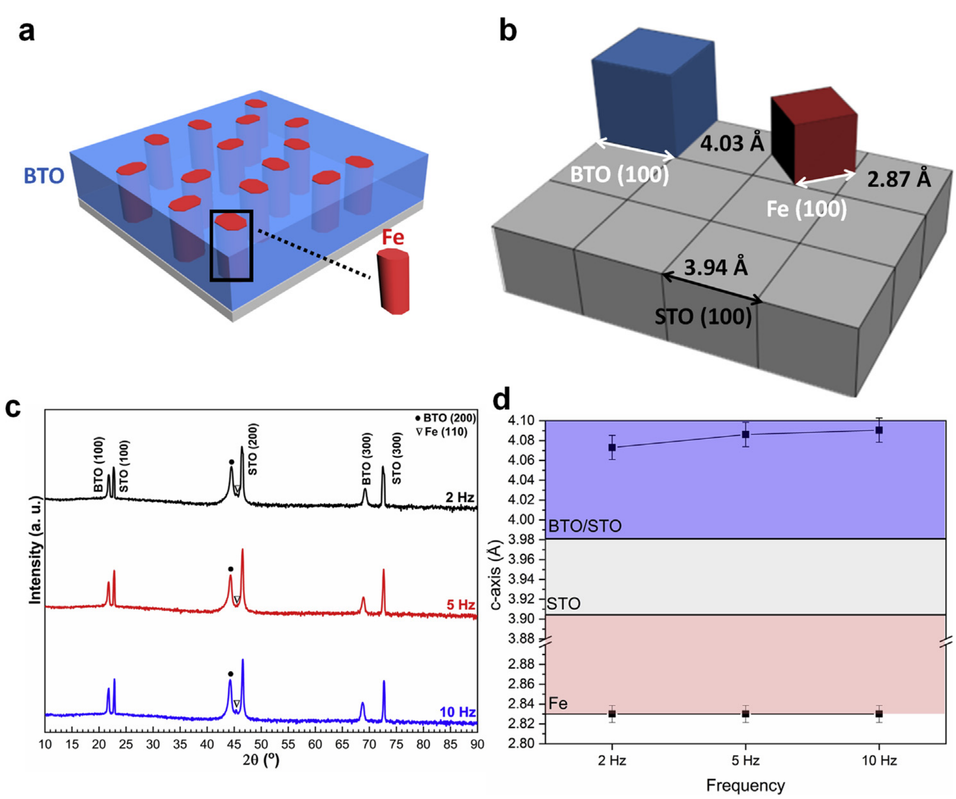

Fig. 1. (a) Schematic demonstrating the proposed growth of Fe pillars within a BTO matrix. (b) Schematic showing the different lattice parameters of BTO and Fe on STO. (c) Typical θ-2θ XRD scan of the different films deposited at different frequencies. (d) The different lattice parameters for BTO and Fe grown at different frequencies. BTO = $BaTiO_3$; STO = SrTiO3; XRD = X-ray diffraction.

microscopy. Magnetoelectrical (ME) coupling was measured using a magnetoelectric bundle (Radiant Technologies, Inc.).

Dielectric permittivity was calculated using a spectroscopic ellipsometer (JA Woollam RC2), with an anisotropic model to fit the ellipsometer parameters ψ and Δ. The IP permittivity was modeled using two Lorentz oscillators, whereas OP permittivity was modeled using a Drude-Lorentz model to enforce Kramers-Kronig consistency.

3. Results and discussion

3.1. X-ray diffraction

θ−2θ XRD scanning was first performed on the Fe-BTO VAN thin films grown under different laser frequencies (2 Hz, 5 Hz, and 10 Hz) to investigate the material composition and the phase distribution. From the XRD data, BTO (001) and STO (001) peaks can readily be identified from Fig. 1c in all samples indicating (00l) BTO texturing on the (00l) STO substrate. In addition, for all samples, the Fe (110) peaks exist at a 2θ value of 45.3° corresponding to a d-spacing of 2.00 Å, indicating a compressive strain of 1.3% compared with reported bulk Fe d-spacing (PDF card# 06-0696) of 2.0268 Å. Meanwhile, the BTO (200) peaks shifts from 44.45° to 44.3° to 44.25° for the 2, 5, and 10 Hz samples, respectively, corresponding to a tensile strain of 2.3%, 2.7%, and 2.8% when compared with the measured BTO (200) peak located at 45.55° in pure BTO/STO samples, with the lattice parameter as seen in Fig. 1b. This highly strained state is created via the two different materials within the metallic VAN forming distinct areas and hints at a strong interface strain between Fe and BTO, with the strong BTO tensile strain compensating for the large Fe compressive strain. In addition, as the laser frequency varies, the BTO peak position shifts, indicating a morphology change, with the lowest frequency having the least tensile strain and the highest frequency with the highest tensile strain.

3.2. Microscopy analysis

To verify whether the frequencies affected the nanostructure, TEM, STEM, and EDS analyses were conducted. The expected morphology of the Fe-BTO nanocomposite is illustrated in Fig. 2a, wherein uniformly distributed Fe nanopillars grow within a BTO matrix. The plan-view STEM images in Fig. 2b−d demonstrate the excellent epitaxial growth of the film, with the average pillar diameter of around 5 nm. The pillars show an overall shape of a rectangle, with sides being in the {110} plane family and with faceted edges being the (111) planes. Fig. 2e−g presents the chemical composition of the nanocomposite with Fe pillars in the BTO matrix. The rectangular shape with facets can be explained by the strain mapping results using geometrical phase analysis (GPA) in Fig. 2h. The GPA analysis of the individual pillar shows an alternating pattern of strain states between tensile (yellow) and compressive (blue) strain. This alternating strain states serve to minimize the total strain energy of the Fe region with alternating strain states. On a closer look, it reveals that the smaller facets have a singular strain state, with the larger one having a combination, resulting in the faceted rectangular shape.

The cross-sectional images in Fig. 2i of the Fe-BTO film demonstrate the high uniformity and high density of the Fe pillars within the BTO matrix, and on further investigation, they demonstrate highly oriented growth, with the pillars growing in a vertical fashion throughout the film thickness. To demonstrate phase separation, EDS mappings in Fig. 2j again confirm the pillars throughout the film thickness were indeed pure Fe, not iron oxide. This is significant owing to the high susceptibility that different metals—especially ferromagnetic ones such as Fe, Ni, and Co—are likely to oxidize. For Fe, the oxidation process is highly detrimental to physical properties, e.g., resulting in smaller coercive fields, magnetic saturation, and a critical temperature significantly lower than room temperature. In addition, from the plan-view images, it is possible to ascertain the high density of Fe regions that exist with the Fe-BTO film and the uniformity of the distribution throughout the film. This regular distribution is highly sought after for future device applications, allowing for easier fabrication of device arrays. The Fe nanopillars are nearly equally spaced resembling an Fe nanoarray, which could be patterned as arrays of spintronic devices.

To further investigate the underlying growth mechanisms of the Fe-BTO hybrid film, different laser frequencies of 2 Hz, 5 Hz, and 10 Hz were used to grow the Fe-BTO films. In the TEM plan-view images in Fig. 3b−k, it is noted that as frequency increases, Fe dimension changed from isotropic morphology to elongated rectangles and then again to squares. While there is a typical Gaussian distribution for the 5-Hz and the 10-Hz samples, the 2-Hz sample does not present such distribution. Instead, it shows a bimodal distribution of nanopillar diameters, i.e., the mixture of large-and small-diameter nanopillars. Such non-uniform nanopillar diameters might be attributed to the non-optimum growth and incomplete nucleation owing to the insufficient flux of Fe adatoms under 2 Hz. This leads to the formation of small nuclei of Fe nanopillars in Fig. 3b−d. The 5-Hz sample has unique rectangular shaped nanopillars with preferred orientation along the IP direction of BTO [010]. The preferred orientation suggests that there is an underlying factor during the growth and nucleation of the Fe adatoms within the Fe-BTO film. One possible explanation may be the interaction between the lattice strain and the adatom diffusion process. When frequency decreases, the adatom diffusion time increases, and the adatoms have sufficient time to diffuse in both the (110) directions, producing an elongated, faceted, rectangular, IP morphology in the 2-Hz sample. For the 5-Hz sample, the diffusion time is in the range allowing the perfect alignment along a preferred crystallographic plane of [020]. This alignment mainly arises from interactions between the surface energies of the Fe, BTO, and STO substrate and the growth kinetics, which mainly include the incoming flux of adatoms and the nucleation and diffusion of the adatoms. More specifically, diffusion of the adatoms and the perfect nucleation/growth of the adatoms have been achieved under the 5-Hz growth condition. The strain compensation model suggests that Fe (a = 0.287 nm) and BTO (a = 0.483 nm) present opposite strain states compared with the STO substrate (a = 0.394 nm). Such IP strain compensation leads to the highly ordered, uniform distribution of Fe nanopillars within the BTO matrix. Such a strain compensation model can be best demonstrated in perfect epitaxial growth of 2-phase VAN systems. Thus, highly ordered and aligned Fe nanopillar distribution has been achieved in the 5-Hz sample. However, the 2-Hz sample clearly shows both very small nanopillars and regular-sized nanopillars (a bimodel distribution), which suggest that there might be insufficient Fe adatoms under the 2-Hz condition and thus leads to various nanopillar diameters. Although 10 Hz leads to high growth rate, it could cause deterioration of epitaxial quality and pillar distribution.

3.3. Physical properties

To investigate how Fe nanostructures with the BTO matrix affect the magnetic and optical properties, magnetization measurements and ellipsometry measurements were conducted, and the data are summarized in Fig. 4. The room-temperature ferromagnetic properties for both the OP and the IP were measured and plotted in

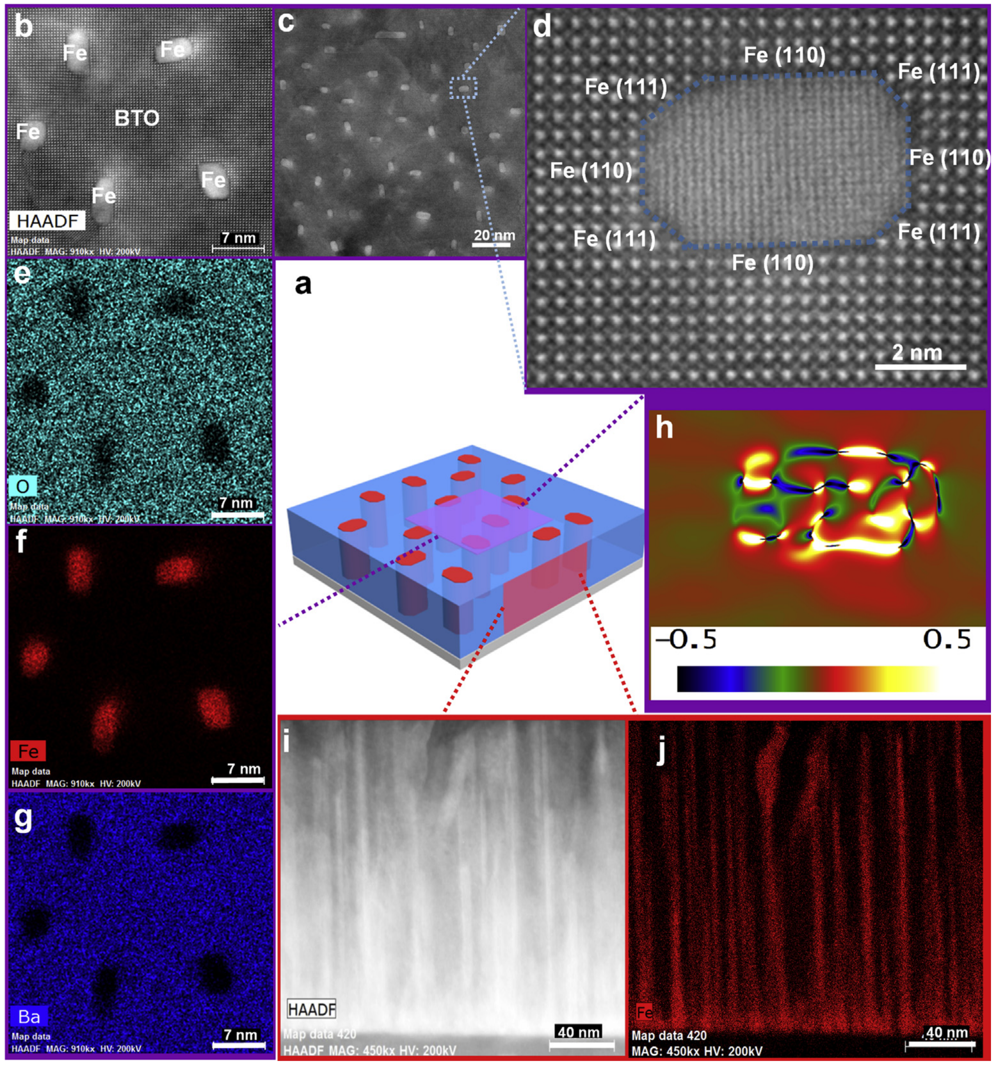

Fig. 2. (a) Schematic demonstrating the Fe-BTO film grown on STO. (b–d) Plan-view STEM images of Fe-BTO grown at 10 Hz. EDS mapping of the plan-view images of Fe-BTO with (e) O, (f) Fe, and (g) Ba mapping shown. (h) GPA analysis of a single pillar to illustrate the strain distribution. (i and j) The STEM and Fe EDS mapping, respectively, of a cross-sectional view. BTO = $BaTiO_3$; STO = $SrTiO_3$;; STEM = scanning transmission electron microscopy; EDS = energy dispersive X-ray spectroscopy; GPA = geometrical phase analysis, HAADF = High-angle annular dark-field .

Fig. 4a and b, respectively. The data show an obvious anisotropy with the OP saturation magnetization of 110 emu/cm^3 and the IP saturation of 70–80 emu/cm^3. In the OP direction, a clear coercive field difference is seen, with the 2-Hz sample having the highest coercive field and the 10-Hz sample having the lowest coercive field value. In addition, the IP direction shows a similar trend as that of the OP results, and the overall coercive field results are plotted in Fig. 4e. Fe-BTO not only has strong tunable ferromagnetic properties but also possesses highly anisotropic dielectric properties owing to its inherent column shape of nanostructures causing a similar column shape of BTO. From the real part of dielectric permittivity, shown in Fig. 4f, it shows that the IP dielectric permittivity value is significantly higher (between 1.5- and 2-fold) than that of the OP direction. In addition,the growth frequency and the dielectric constants haveseem to be correlated in that as the frequency decreases, the dielectric constant also decreases. These trends can be explained from morphology tuning. As frequency decreases, adatom diffusion increases and the dimension of the Fe nanopillars increases. If each Fe region is taken as a single magnetic domain, as length increases, the required energy to saturate and bias the magnetic moment of the Fe region increases with size. In addition, it has been previously reported that the superparamagnetic limit of Fe nanoparticles is around 10 nm [47]. Although the Fe pillars have a diameter of less than 10 nm, they may still be ferromagnetic owing to their pillar-type morphology. As the diameter increases above the limit, coercivity of Fe increases, which affects the IP and OP coercivity. The 2-Hz Fe-BTO sample has a larger coercive field owing to the existence of several larger lateral Fe domains that may be affecting the magnetization of neighboring pillars. As in the case of the saturation magnetic values,since the concentration of the Fe remains constant at 1:1 for the Fe to BTO ratio and all the different frequencies were grown with comparable film thicknesses, similar amounts of Fe will be found within all the films, resulting in similar saturation magnetic values In a similar manner the diameter affects the magnetic behavior, the optical property is also affected. As the pillars elongate in diameter, there will be more metallic characteristics leading to a lower overall dielectric constant of the system in both the IP and OP directions. The anisotropy can be explained from the fact that the metals are in pillar fashion; the Fe-BTO system will behave more metallic in the OP direction, resulting in a lower permittivity than that of the IP direction. Overall, the fact that varying deposition frequency was

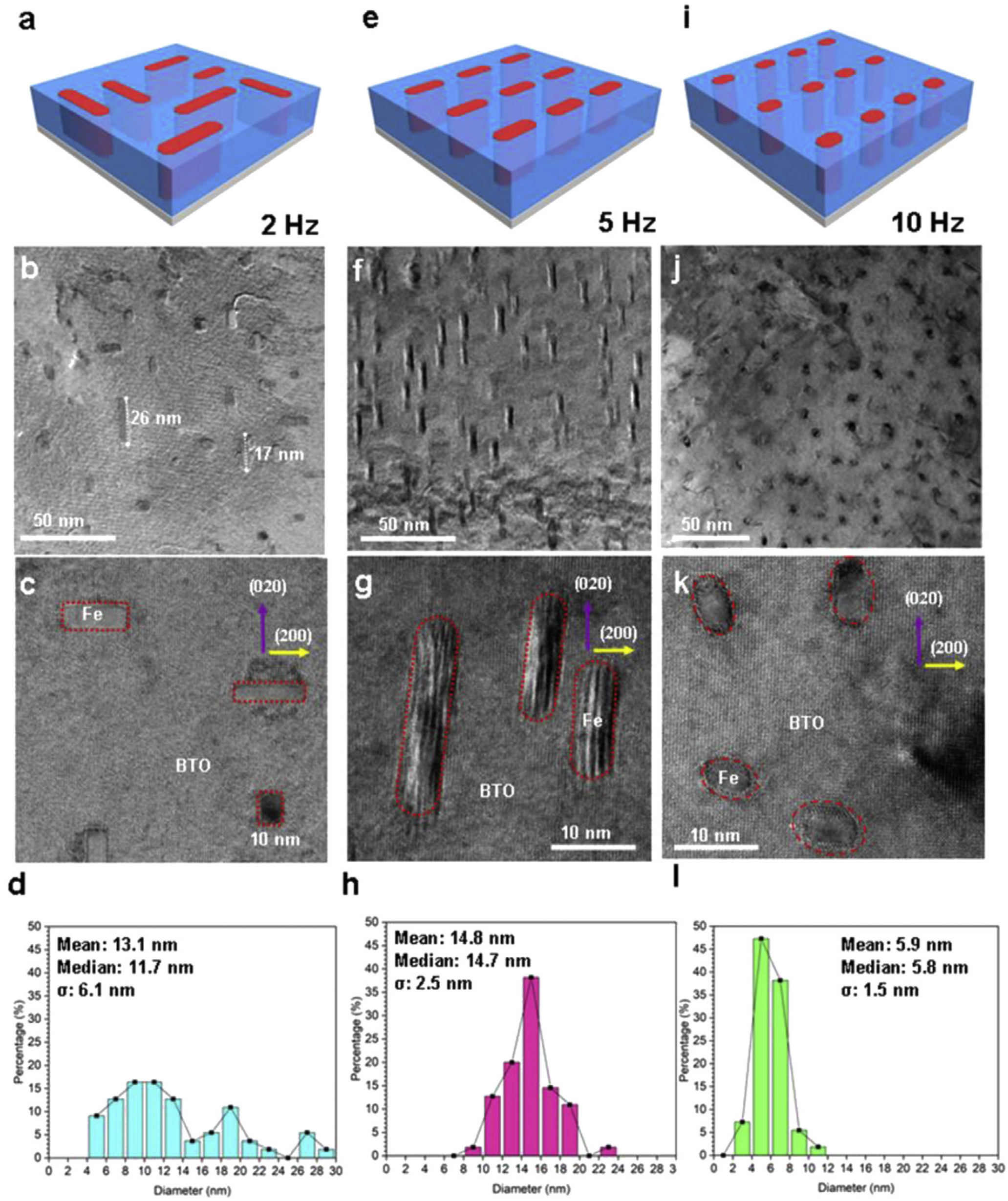

Fig. 3. (a, e, and i) Schematic demonstrating the how pillar diameters vary with different frequencies. (b, c, f, g, j, and k) Plan-view TEM images demonstrating the pillar variation. (d, h, and l) Histogram plots illustrating the nanopillar diameter distribution for the samples deposited under different laser frequencies. TEM = transmission electron microscopy.

able to tune both the optical and ferromagnetic behaviors further highlights the potential of the unique Fe-BTO VAN systems for future optical and magnetic device applications.

3.4. Demonstration of the multiferroic properties

To demonstrate the potential multifunctionality of the Fe-BTO film, a multilayer stack was grown, with BTO encapsulating the Fe-BTO film to electrically isolate the Fe regions from the conductive bottom $La_{0.7}Sr_{0.3}MnO_3$ (LSMO) layer, as shown in Fig. 5. It is clear that the BTO region isolated the Fe portions from the semimetal LSMO, facilitating the polarization of the BTO regions in the Fe-BTO nanocomposite. This configuration allows for room-temperature ferroelectric and ferromagnetic properties to occur within the device. As shown in Fig. 5, it is possible to see the different ferromagnetic and ferroelectric properties to confirm that the multilayer device has both properties. The ferromagnetic properties also show anisotropy with the coercive field, differing from the OP and IP directions. Compared with the single-layer Fe/BTO films, wherein Fe and BTO are grown in layers on top of one another, the properties show OP anisotropy, as seen in the ferromagnetic and optical data, demonstrating anisotropic ferromagnetic and ferroelectric properties. This multistack configuration allows for two main applications compared with the single-layer film: isolating the metallic regions for individual biasing of different metal pillars, creating local electrical polarization and switching, and room-temperature magnetic switching throughout the film. In addition, the weak ferromagnetic properties and weak ferroelectricity will affect each other, causing highly anisotropic, room-temperature coupling of both electrical and magnetic properties. To further investigate the coupling, a ME coupling measurement was performed, with the results plotted in Fig. S1. In the plot, a black line shows the linear

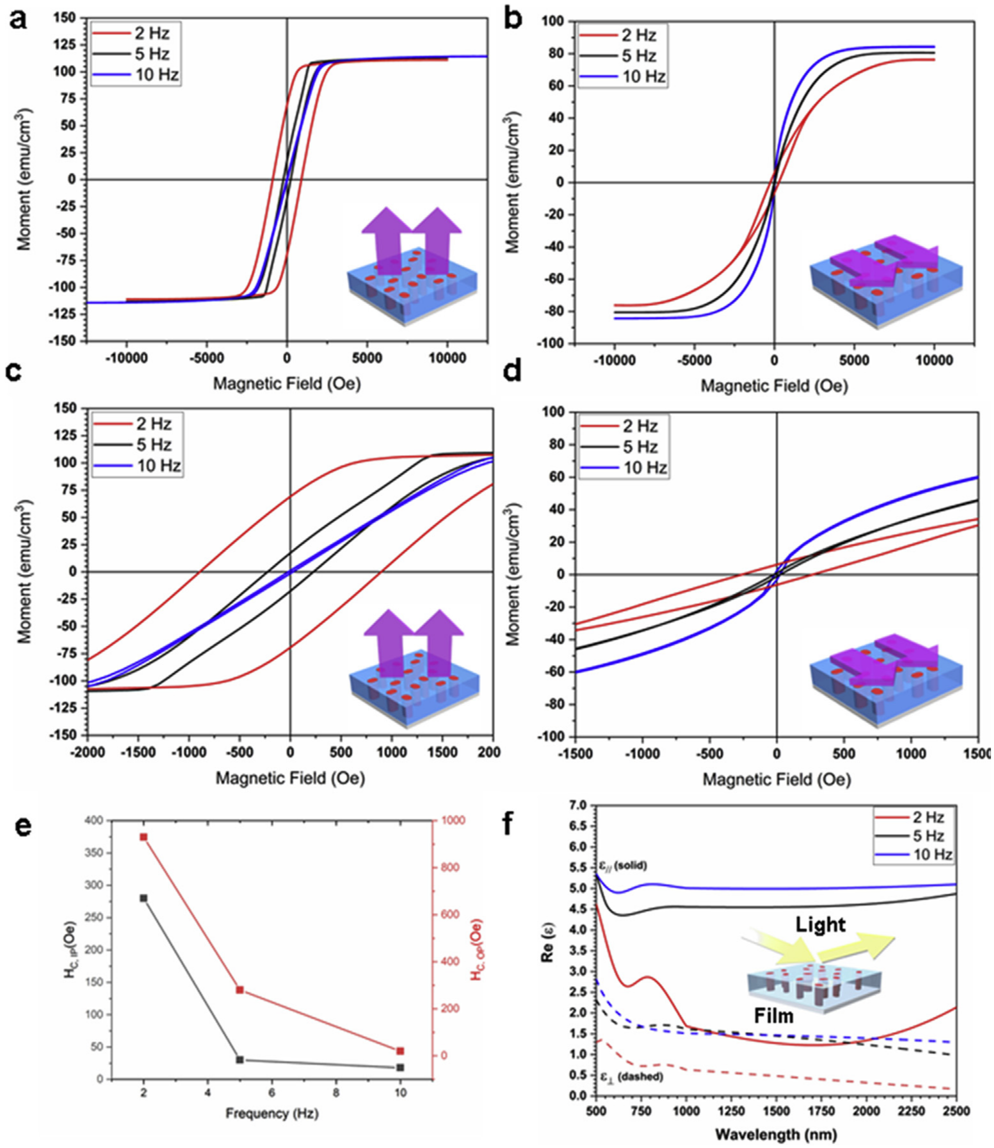

Fig. 4. (a and b) Hysteresis loops of the Fe-BTO films grown at different frequencies with (c and d) graphs magnifying the magnetic moments around the coercivities. (e) Graph depicting the variation of the coercivities when the field is applied in both the in-plane and out-of-plane directions as a function of the deposition frequency. (f) Different dielectric constants of the different frequencies as modeled using data from the ellipsometer. BTO = $BaTiO_3$.

fitting analysis, with the slope indicating a ME charge coefficient, α, of around 1.02×10^{-4} $\mu C/(cm^2\ Oe)$. Because the ferroelectric properties and polarization mainly come from BTO, a previously reported, room-temperature relative permittivity of BTO was used [48]. The calculated ME voltage coefficient is 2.30 V/(cm Oe). Owing to magnetization limitations, the slope does not change in the measured range. This coupling creates new avenues for potential applications in spintronics and the stochastic computing scheme.

4. Conclusions

This study demonstrates the growth of Fe nanopillar arrays within a BTO matrix with room-temperature multiferroic properties. By tuning the growth parameters, it is possible to modify the nanostructure, and effectively tune the strain and the magnetic properties. This study found that lower deposition frequencies result in Fe pillars with larger diameters, both lower vertical strain coupling and higher magnetic coercive fields; whereas for higher frequencies, it leads to smaller pillar diameters, higher vertical strain coupling, and lower coercive fields. Furthermore, to demonstrate the potential of room-temperature multiferroic nanocomposites, a multilayer stack with an encapsulated Fe-BTO layer was shown to demonstrate the potential by electrically isolating the Fe regions from one another, aiding the polarization of the ferroelectric BTO regions. This Fe-BTO VAN film presents a platform for highly anisotropic, room-temperature multiferroic properties, with a wide range of tunability for various electrical, magnetic, and optical devices.

Declaration of competing interest

The authors declare that they have no known competing financial interests or personal relationships that could have appeared to influence the work reported in this paper.

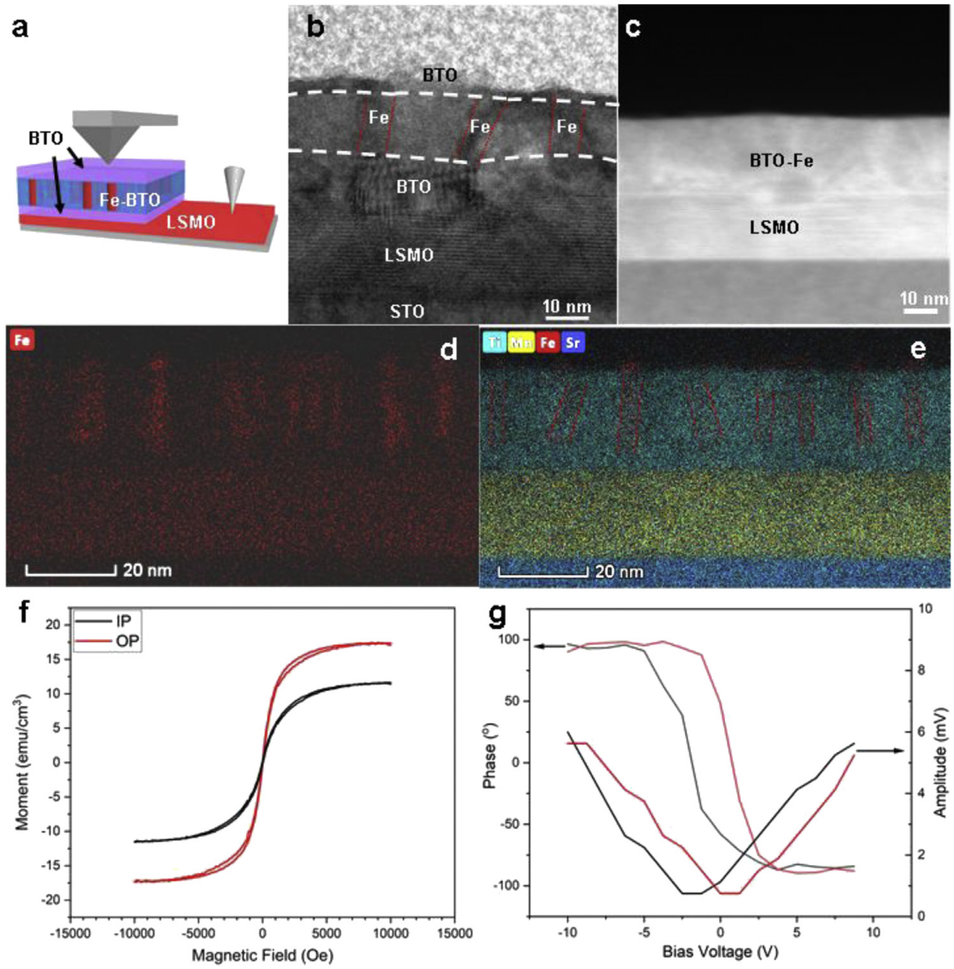

Fig. 5. (a) Schematic of the multilayer used to isolate the Fe regions within the film from the bottom conductor. (b) TEM and (c) STEM images of the multilayer. (d and e) EDS mapping of the multilayer with the (f) ferromagnetic and (g) ferroelectric properties. TEM = transmission electron microscopy; STEM = scanning transmission electron microscopy; BTO = $BaTiO_3$; STO = $SrTiO_3$; LSMO = La0.7Sr0.3MnO$_3$; EDS = energy dispersive X-ray spectroscopy; IP = in-plane; OP = out-of-plane.

CRediT authorship contribution statement

B. Zhang: Conceptualization, Methodology, Formal analysis, Writing - original draft. **J. Huang:** Conceptualization, Methodology, Validation. **B.X. Rutherford:** Visualization, Writing - review & editing, Investigation. **P. Lu:** Investigation, Visualization. **S. Misra:** Investigation, Formal analysis, Writing - review & editing. **M. Kalaswad:** Investigation, Writing - review & editing. **Z. He:** Investigation. **X. Gao:** Investigation, Formal analysis. **X. Sun:** Investigation. **L. Li:** Investigation. **H. Wang:** Writing - review & editing, Project administration, Supervision, Funding acquisition, Resources.

Acknowledgments

This work was supported by the US Department of Energy, Office of Science, Basic Energy Sciences under Awardaward DE-SC0020077. The electrical testing effort at Purdue University was supported by the US National Science Foundation (ECCS-1902644). The high-resolution transmission electron microscopy/scanning transmission electron microscopy characterization at Purdue University was supported by the US National Science Foundation (DMR-1565822). Sandia National Laboratories is a multiprogram laboratory managed and operated by National Technology and Engineering Solutions of Sandia, LLC, a wholly owned subsidiary of Honeywell International, Inc., for the U.S. Department of Energy's National Nuclear Security Administration under contract DE-NA0003525. This paper describes objective technical results and analysis. Any subjective views or opinions that might be expressed in the paper do not necessarily represent the views of the U.S. Department of Energy or the United States Government.

Appendix A. Supplementary data

Supplementary data to this article can be found online at https://doi.org/10.1016/j.mtnano.2020.100083.

References

[1] B. Tudu, A. Tiwari, Recent developments in perpendicular magnetic anisotropy thin films for data storage applications, Vacuum 146 (2017) 329–341, https://doi.org/10.1016/j.vacuum.2017.01.031.
[2] S.A. Wolf, Spintronics: a spin-based electronics vision for the future, Science (80-.) 294 (2001) 1488–1495, https://doi.org/10.1126/science.1065389.
[3] I. Žutić, J. Fabian, S. Das Sarma, Spintronics: fundamentals and applications, Rev. Mod. Phys. 76 (2004) 323–410, https://doi.org/10.1103/RevModPhys.76.323.
[4] K. Tarawneh, N. Al-Aqtash, R. Sabirianov, Large magnetoresistance in planar Fe/MoS2/Fe tunnel junction, Comput. Mater. Sci. 124 (2016) 15–22, https://doi.org/10.1016/j.commatsci.2016.06.005.
[5] X.-G. Zhang, W.H. Butler, A. Bandyopadhyay, Effects of the iron-oxide layer in Fe-FeO-MgO-Fe tunneling junctions, Phys. Rev. B 68 (2003) 6–9, https://doi.org/10.1103/PhysRevB.68.092402.

[6] J. Mathon, A. Umerski, Theory of tunneling magnetoresistance of an epitaxial Fe/MgO/Fe(001) junction, Phys. Rev. B - Condens. Matter Mater. Phys. 63 (2001) 1–4, https://doi.org/10.1103/PhysRevB.63.220403.

[7] H. Liu, D. Bedau, D. Backes, J.A. Katine, J. Langer, A.D. Kent, Ultrafast switching in magnetic tunnel junction based orthogonal spin transfer devices, Appl. Phys. Lett. 97 (2010) 242510, https://doi.org/10.1063/1.3527962.

[8] L. López-Mir, C. Frontera, H. Aramberri, K. Bouzehouane, J. Cisneros-Fernández, B. Bozzo, L. Balcells, B. Martínez, Anisotropic sensor and memory device with a ferromagnetic tunnel barrier as the only magnetic element, Sci. Rep. 8 (2018) 1–10, https://doi.org/10.1038/s41598-017-19129-5.

[9] J. Huang, Z. Qi, L. Li, H. Wang, S. Xue, B. Zhang, X. Zhang, H. Wang, Self-assembled vertically aligned Ni nanopillars in CeO2with anisotropic magnetic and transport properties for energy applications, Nanoscale 10 (2018) 17182–17188, https://doi.org/10.1039/c8nr05532g.

[10] J. Huang, L. Li, P. Lu, Z. Qi, X. Sun, X. Zhang, H. Wang, Self-assembled Co-BaZrO3nanocomposite thin films with ultra-fine vertically aligned Co nanopillars, Nanoscale 9 (2017) 7970–7976, https://doi.org/10.1039/c7nr01122a.

[11] J.L. Macmanus-Driscoll, Self-assembled heteroepitaxial oxide nanocomposite thin film structures: designing interface-induced functionality in electronic materials, Adv. Funct. Mater. 20 (2010) 2035–2045, https://doi.org/10.1002/adfm.201000373.

[12] J.L. MacManus-Driscoll, P. Zerrer, H. Wang, H. Yang, J. Yoon, A. Fouchet, R. Yu, M.G. Blamire, Q. Jia, Strain control and spontaneous phase ordering in vertical nanocomposite heteroepitaxial thin films, Nat. Mater. 7 (2008) 314–320, https://doi.org/10.1038/nmat2124.

[13] W. Zhang, M. Fan, L. Li, A. Chen, Q. Su, Q. Jia, J.L. MacManus-Driscoll, H. Wang, Heterointerface design and strain tuning in epitaxial BiFeO 3 :CoFe 2 O 4 nanocomposite films, Appl. Phys. Lett. 107 (2015) 212901, https://doi.org/10.1063/1.4936157.

[14] X. Gao, L. Li, J. Jian, H. Wang, M. Fan, J. Huang, X. Wang, H. Wang, Vertically aligned nanocomposite BaTiO3:YMnO3 thin films with room temperature multiferroic properties toward nanoscale memory devices, ACS Appl. Nano Mater. 1 (2018) 2509–2514, https://doi.org/10.1021/acsanm.8b00614.

[15] W. Zhang, M. Fan, L. Li, A. Chen, Q. Su, Q. Jia, J.L. MacManus-Driscoll, H. Wang, Heterointerface design and strain tuning in epitaxial BiFeO 3 :CoFe 2 O 4 nanocomposite films, Appl. Phys. Lett. 107 (2015) 212901, https://doi.org/10.1063/1.4936157.

[16] A. Chen, Z. Bi, Q. Jia, J.L. Macmanus-Driscoll, H. Wang, Microstructure, vertical strain control and tunable functionalities in self-assembled, vertically aligned nanocomposite thin films, Acta Mater. 61 (2013) 2783–2792, https://doi.org/10.1016/j.actamat.2012.09.072.

[17] A. Chen, Z. Harrell, P. Lu, E. Enriquez, L. Li, B. Zhang, P. Dowden, C. Chen, H. Wang, J.L. MacManus-Driscoll, Q. Jia, Strain enhanced functionality in a bottom-up approach enabled 3D super-nanocomposites, Adv. Funct. Mater. 1900442 (2019) 1–8, https://doi.org/10.1002/adfm.201900442.

[18] M. Fan, W. Zhang, J. Jian, J. Huang, H. Wang, Strong perpendicular exchange bias in epitaxial La 0.7 Sr 0.3 MnO 3 :LaFeO 3 nanocomposite thin films, Apl. Mater. 4 (2016), 076105, https://doi.org/10.1063/1.4958965.

[19] W.R. Zhang, A.P. Chen, J. Jian, Y.Y. Zhu, L. Chen, P. Lu, Q.X. Jia, J.L. MacManus-Driscoll, X.H. Zhang, H.Y. Wang, Strong perpendicular exchange bias in epitaxial La0.7Sr0.3MnO3:BiFeO3 nanocomposite films through vertical interfacial coupling, Nanoscale 7 (2015) 13808–13815, https://doi.org/10.1039/c5nr03231h.

[20] W. Zhang, L. Li, P. Lu, M. Fan, Q. Su, F. Khatkhatay, A. Chen, Q. Jia, X. Zhang, J.L. MacManus-Driscoll, H. Wang, Perpendicular exchange-biased magnetotransport at the vertical heterointerfaces in La0.7Sr0.3MnO3:NiO nanocomposites, ACS Appl. Mater. Interfaces. 7 (2015) 21646–21651, https://doi.org/10.1021/acsami.5b06314.

[21] Q. Su, W. Zhang, P. Lu, S. Fang, F. Khatkhatay, J. Jian, L. Li, F. Chen, X. Zhang, J.L. Macmanus-Driscoll, A. Chen, Q. Jia, H. Wang, Self-assembled magnetic metallic nanopillars in ceramic matrix with anisotropic magnetic and electrical transport properties, ACS Appl. Mater. Interfaces 8 (2016) 20283–20291, https://doi.org/10.1021/acsami.6b05999.

[22] B. Zhang, M. Fan, L. Li, J. Jian, J. Huang, H. Wang, M. Kalaswad, H. Wang, Tunable magnetic anisotropy of self-assembled Fe nanostructures within a La0.5Sr0.5FeO3 matrix, Appl. Phys. Lett. 112 (2018), https://doi.org/10.1063/1.5008382, 0–5.

[23] L. Li, L. Sun, J.S. Gomez-Diaz, N.L. Hogan, P. Lu, F. Khatkhatay, W. Zhang, J. Jian, J. Huang, Q. Su, M. Fan, C. Jacob, J. Li, X. Zhang, Q. Jia, M. Sheldon, A. Alù, X. Li, H. Wang, Self-assembled epitaxial Au-oxide vertically aligned nanocomposites for nanoscale metamaterials, Nano Lett. 16 (2016) 3936–3943, https://doi.org/10.1021/acs.nanolett.6b01575.

[24] B. Zhang, M. Fan, L. Li, J. Jian, J. Huang, H. Wang, M. Kalaswad, H. Wang, Tunable magnetic anisotropy of self-assembled Fe nanostructures within a La 0.5 Sr 0.5 FeO 3 matrix, Appl. Phys. Lett. 112 (2018), 013104, https://doi.org/10.1063/1.5008382.

[25] L. Li, L. Sun, J.S. Gomez-Diaz, N.L. Hogan, P. Lu, F. Khatkhatay, W. Zhang, J. Jian, J. Huang, Q. Su, M. Fan, C. Jacob, J. Li, X. Zhang, Q. Jia, M. Sheldon, A. Alu, X. Li, H. Wang, Self-assembled epitaxial Au-oxide vertically aligned nanocomposites for nanoscale metamaterials, NANO Lett 16 (2016) 3936–3943, https://doi.org/10.1021/acs.nanolett.6b01575.

[26] S. Misra, L. Li, J. Jian, J. Huang, X. Wang, D. Zemlyanov, J.W. Jang, F.H. Ribeiro, H. Wang, Tailorable Au nanoparticles embedded in epitaxial TiO2 thin films for tunable optical properties, ACS Appl. Mater. Interfaces 10 (2018) 32895–32902, https://doi.org/10.1021/acsami.8b12210.

[27] J. Huang, J.L. MacManus-Driscoll, H. Wang, New epitaxy paradigm in epitaxial self-assembled oxide vertically aligned nanocomposite thin films, J. Mater. Res. 32 (2017) 4054–4066, https://doi.org/10.1557/jmr.2017.281.

[28] K.J. Choi, M. Biegalski, Y.L. Li, A. Sharan, J. Schubert, R. Uecker, P. Reiche, Y.B. Chen, X.Q. Pan, V. Gopalan, L.-Q. Chen, D.G. Schlom, C.B. Eom, Enhancement of ferroelectricity in strained BaTiO3 thin films-supplementary info, Science 306 (2004) 1005–suppl, https://doi.org/10.1126/science.1103218.

[29] L. Huang, Z. Chen, J.D. Wilson, S. Banerjee, R.D. Robinson, I.P. Herman, R. Laibowitz, S. O'Brien, Barium titanate nanocrystals and nanocrystal thin films: synthesis, ferroelectricity, and dielectric properties, J. Appl. Phys. 100 (2006), 034316, https://doi.org/10.1063/1.2218765.

[30] M. Dawber, K.M. Rabe, J.F. Scott, Physics of thin-film ferroelectric oxides, Rev. Mod. Phys. 77 (2005) 1083–1130, https://doi.org/10.1103/RevModPhys.77.1083.

[31] V.N. Reddy, K.C. Babu Naidu, T. Subbarao, Structural, optical and ferroelectric properties of BaTiO3 ceramics, J. Ovonic Res. 12 (2016) 185–191.

[32] V. Mishra, A. Sagdeo, V. Kumar, M.K. Warshi, H.M. Rai, S.K. Saxena, D.R. Roy, V. Mishra, R. Kumar, P.R. Sagdeo, Electronic and optical properties of BaTiO 3 across tetragonal to cubic phase transition: an experimental and theoretical investigation, J. Appl. Phys. 122 (2017), 065105, https://doi.org/10.1063/1.4997939.

[33] L.A. Wills, B.W. Wessels, D.S. Richeson, T.J. Marks, Epitaxial growth of BaTiO3 thin films by organometallic chemical vapor deposition, Appl. Phys. Lett. 60 (1992) 41–43, https://doi.org/10.1063/1.107359.

[34] T. Woldu, B. Raneesh, P. Sreekanth, M.V. Ramana Reddy, R. Philip, N. Kalarikkal, Size dependent nonlinear optical absorption in BaTiO3 nanoparticles, Chem. Phys. Lett. 625 (2015) 58–63, https://doi.org/10.1016/j.cplett.2015.02.020.

[35] T. Jin, L. Li, B. Zhang, H.Y.G. Lin, H. Wang, P.T. Lin, Monolithic mid-infrared integrated photonics using silicon-on-epitaxial barium titanate thin films, ACS Appl. Mater. Interfaces. 9 (2017) 21848–21855, https://doi.org/10.1021/acsami.7b02681.

[36] C. Xiong, W.H.P. Pernice, J.H. Ngai, J.W. Reiner, D. Kumah, F.J. Walker, C.H. Ahn, H.X. Tang, Active silicon integrated nanophotonics: ferroelectric BaTiO3 devices, Nano Lett. 14 (2014) 1419–1425, https://doi.org/10.1021/nl404513p.

[37] T. Jin, L. Li, B. Zhang, H.Y.G. Lin, H. Wang, P.T. Lin, Real-time and label-free chemical sensor-on-a-chip using monolithic Si-on-BaTiO3 mid-infrared waveguides, Sci. Rep. 7 (2017) 5836, https://doi.org/10.1038/s41598-017-05711-4.

[38] T. Jin, L. Li, B. Zhang, H.-Y.G. Lin, H. Wang, P.T. Lin, Epitaxial barium titanate thin films for mid-infrared photonic circuits, in: Adv. Photonics 2017 (IPR, NOMA, Sensors, Networks, SPPCom, PS), OSA, Washington, D.C., 2017, https://doi.org/10.1364/iprsn.2017.ith1a.5. ITh1A.5.

[39] G. Venkataiah, Y. Shirahata, M. Itoh, T. Taniyama, Manipulation of magnetic coercivity of Fe film in Fe/BaTiO3 heterostructure by electric field, Appl. Phys. Lett. 99 (2011) 98–101, https://doi.org/10.1063/1.3628464.

[40] G. Venkataiah, Y. Shirahata, I. Suzuki, M. Itoh, T. Taniyama, Strain-induced reversible and irreversible magnetization switching in Fe/BaTiO 3 heterostructures, J. Appl. Phys. 111 (2012), 033921, https://doi.org/10.1063/1.3684695.

[41] Y. Shirahata, T. Nozaki, G. Venkataiah, H. Taniguchi, M. Itoh, T. Taniyama, Switching of the symmetry of magnetic anisotropy in Fe/BaTiO3heterostructures, Appl. Phys. Lett. 99 (2011) 1–4, https://doi.org/10.1063/1.3609237.

[42] S. Brivio, C. Rinaldi, D. Petti, R. Bertacco, F. Sanchez, Epitaxial growth of Fe/BaTiO3 heterostructures, Thin Solid Films 519 (2011) 5804–5807, https://doi.org/10.1016/j.tsf.2010.12.193.

[43] K. Samuvel, K. Ramachandran, Structure, electrical and magnetic property investigations on Fe-doped hexagonal BaTiO3, Optik (Stuttg). 127 (2016) 1781–1786, https://doi.org/10.1016/j.ijleo.2015.10.240.

[44] W.A. Borders, A.Z. Pervaiz, S. Fukami, K.Y. Camsari, H. Ohno, S. Datta, Integer factorization using stochastic magnetic tunnel junctions, Nature 573 (2019) 390–393, https://doi.org/10.1038/s41586-019-1557-9.

[45] M.L. Schneider, C.A. Donnelly, S.E. Russek, B. Baek, M.R. Pufall, P.F. Hopkins, P.D. Dresselhaus, S.P. Benz, W.H. Rippard, Ultralow power artificial synapses using nanotextured magnetic josephson junctions, Sci. Adv. 4 (2018), https://doi.org/10.1126/sciadv.1701329.

[46] K. Yue, Y. Liu, R.K. Lake, A.C. Parker, A brain-plausible neuromorphic on-the-fly learning system implemented with magnetic domain wall analog memristors, Sci. Adv. 5 (2019) 1–10, https://doi.org/10.1126/sciadv.aau8170.

[47] D.L. Huber, Synthesis, properties, and applications of iron nanoparticles, Small 1 (2005) 482–501, https://doi.org/10.1002/smll.200500006.

[48] B.H. Hoerman, G.M. Ford, L.D. Kaufmann, B.W. Wessels, Dielectric properties of epitaxial BaTiO3 thin films, Appl. Phys. Lett. 73 (1998) 2248–2250, https://doi.org/10.1063/1.121691.